Available online www.jsaer.com

***Journal of Scientific and Engineering Research*, 2016, 3(3):367-376**

Research Article

ISSN: 2394-2630
CODEN(USA): JSERBR

Fracture and Fatigue Crack Growth Characterization of Conventional and Head Hardened Railway Rail Steels

Ali Motameni, Ahmet N Eraslan

Department of Engineering Sciences, Middle East Technical University, Ankara, Turkey

Abstract Today in urban and interurban transport, railways are preferred due to safety, speed and comfort they suggest. With the development of high speed railway systems the time needed for journeys decreased significantly. Increase in train performance and rail traffic necessitated the development of new grades of materials used in the construction of rails. With development of high speed trains, rail-wheel interface stresses increased. So, rolling contact fatigue (RCF) defects like head checks and especially wear became more substantial. Newly developed head hardened rail steel have better resistance against RCF defects than conventional rail steels. Furthermore, head hardened pearlitic rail steels exhibit better wear performance compared to conventional pearlitic rail steels. In parallel to wear and rolling contact fatigue (RCF), fatigue crack propagation (FCG) and fracture of railway components have a great important issue for safety. In this study, mode I fatigue crack propagation and fracture behavior of rail R350 HT grade rail steel compared to conventional R260 grade rail steel in head, web and foot of rail.

Keywords Fatigue crack propagation (FCG), Fracture, Rolling Contact Fatigue (RCF), Wear

Introduction

With the beginning of high speed trains, higher axle loads and increased volume of traffic, rolling contact fatigue (RCF) defects and wear of rail became so crucial [1]. For an axle load of 25 tons at the running of the rail, wheel rail contact stresses typically can reach to 1500 MPa [2]. Together with wear and RCF, reliable damage tolerance design have to be maintained with taking into account fracture and fatigue crack propagation of rails [3]. In last two decades, manufacturer of rail steel focused on improving rail steel have higher hardness value since it is taught that hardness directly relates to wear [4]. Naturally cooled conventional rails grade (R260 and 200) have pearlitic microstructure. In pearlite, arrangement of lamellae of iron and iron carbide, grain size and inter-lamellar spacing have a big role in the hardness of the rail steel. Decreasing inter-lamellar spacing and grain size of peralite structure bring about higher hardness in the rail steel [5]. To achieve this, naturally cooled rails have coarse lamella spacing with low value of hardness approximately about 300 Brinell hardness (HB) improved by controlled cooling rails (Head hardened) have finer inter-lamellar spacing and hence higher value of hardness 340-390 HB.

In this study fracture and fatigue crack growth of naturally cooled rail (R260) and Modern control cooled head hardened (R350 HT) compared in the head, web and foot of rail in transverse direction.

Experimental procedure

Material

In this study, the materials used were 60 kg Head hardened R350 HT and conventional R260 rail steel. Rail were produced by hot rolling directly from an ingot and subsequently cooled by controlled cooling processes to achieve microstructure of interest. Optic and scanning electron microscope micrographs of both rails are shown in Figure 1 and 2. The microstructure of rails consisted of a fully pearlitic structure. Average Inter-lamellar spacing of two rails measured and tabulated in Table 1.

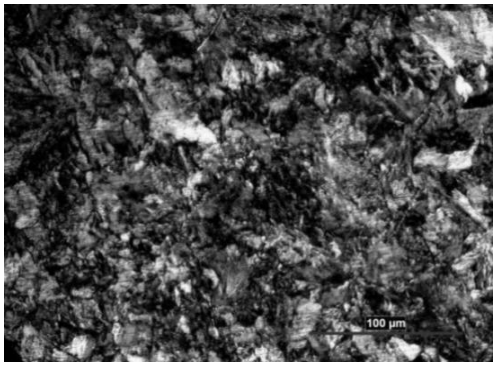

(a)

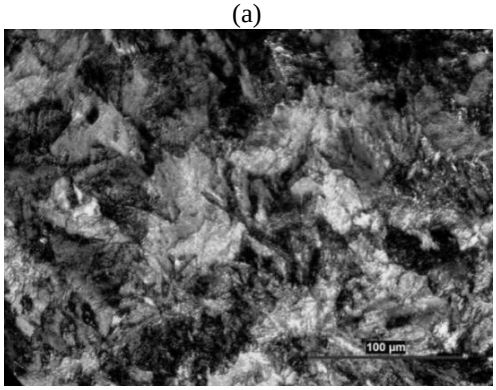

(b)

Figure 1: Micrograph of rail R350 HT and R260 (X200).

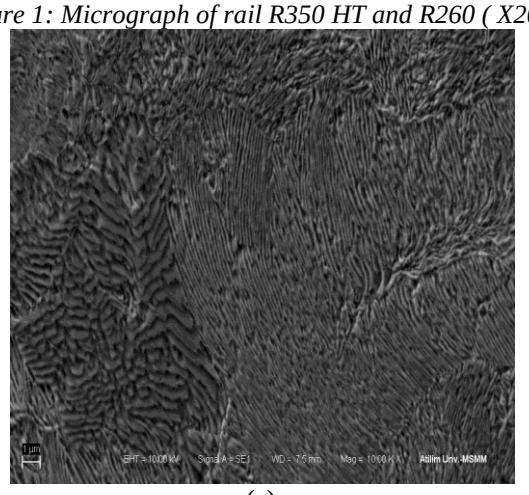

(a)

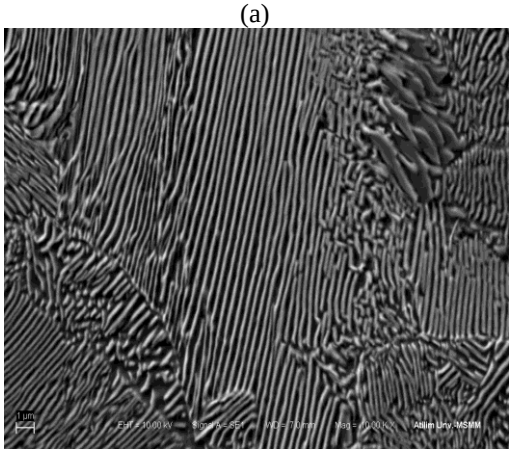

(b)

Figure 2: Micrograph of rail R350 HT and R260 (X10000).

Table 1: Inter lamellar spacing of R350 HT and R260.

Rail Grade	Inter Lamellar Spacing at Different Grains (nm)			Average Inter Lamellar Spacing (nm)
R350 HT	87.08	88.23	83.60	86.30
R260	144.24	201.85	152.69	166.26

The chemical composition and mechanical properties were summarized in Tables 2 and 3, respectively. The tensile tests were performed at a crosshead speed of 1 mm min^{-1} in displacement control. Round tensile specimens with a 8 mm diameter and 40 mm of reduced section were machined in accordance with ASTM E8M [6], oriented in the longitudinal and transverse direction of head.

Table 2: Chemical composition of Rail R350 HT and R260 in weight percentages.

Rail Grade	C	Si	Mn	P	Cr	Fe
R350HT	0.7808	0.4043	1.0597	0.0138	0.0292	97.6400
R260	0.6524	0.2386	1.0685	0.0115	0.0252	97.9400

Table 3(a): Tensile results of R350HT

Specimen No.	Yield Strength *(MPa)*	Tensile Strength *(Mpa)*	Percent longation *(%)*	Percent Reduction in Area *(%)*
L Direction Head	984	1278	9.0	20.7
L Direction Web	605	999	9.7	21.2
T Direction Head	755	1079	20.4	23.7

Table 3(b): Tensile results of R260 rail

Specimen No.	Yield Strength *(MPa)*	Tensile Strength *(Mpa)*	Percent longation *(%)*	Percent Reduction in Area *(%)*
L Direction Head	597	940	18.3	17.3
L Direction Web	473	907	13.7	19.6
T Direction Head	654	926	18.3	17.3

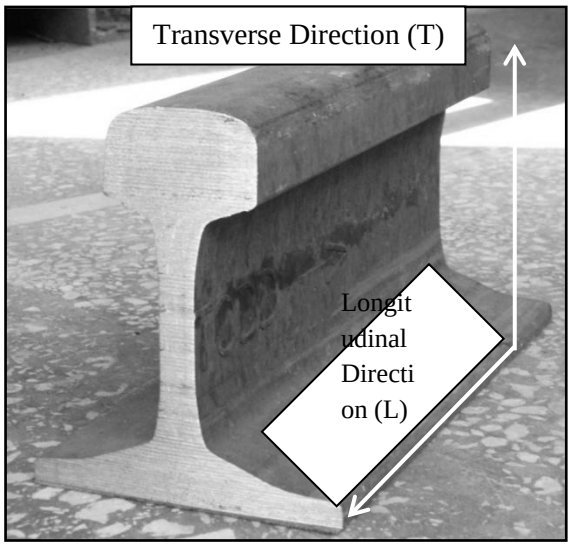

Figure 3: Orientation of specimens machine from rail.

The types of fatigue and fracture specimens were compact tension CT shown in Figure 4. These specimens were cut from rails in the L-T orientation from head, web and foot to model the behavior of transverse crack growth as shown in Figure 3.

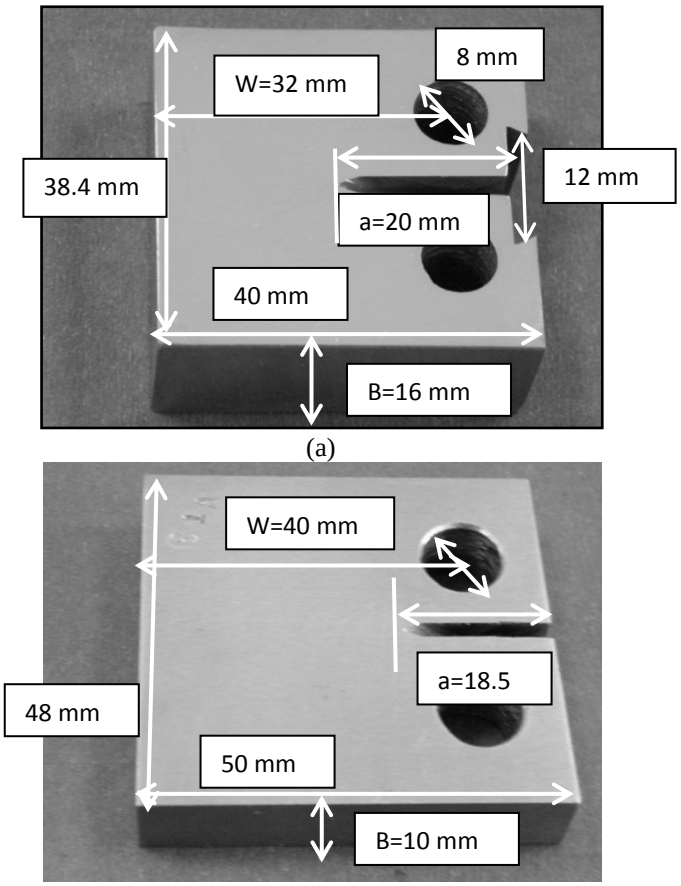

Figure 4: Configuration of test specimens.

Fracture toughness test

Fracture toughness tests were conducted in air at room temperature on a servo-hydraulic test machine (MTS) having a load capacity of 10 tons. Compact tension specimens were precracked until 0.5 W to conform the requirement of the standard (total size of crack starter plus fatigue crack) [7]. Fatigue precrack force selected such that fatigue sinusoidal force cycle does not pass 80 % of the predicted K_{Ic} value of the material, since higher values of K_{max} can cause sudden failure of the specimen and/or high rate of fatigue crack growth. The extension of fatigue precrack until the 0.5 W monitored using traveling microscope with the sensitivity of 0.1 mm.

$$K_Q = \frac{P_Q}{\sqrt{BB_N}\sqrt{W}} f(\frac{a}{w})$$

$$f\left(\frac{a}{w}\right) = \frac{\left(2+\frac{a}{w}\right)\left[0.886+\frac{4.64a}{w}-13.32\left(\frac{a}{w}\right)^2+14.72\left(\frac{a}{w}\right)^3-5.6\left(\frac{a}{w}\right)^4\right]}{\left(1-\frac{a}{w}\right)^{\frac{3}{2}}}$$

Fatigue crack growth rate test

Fatigue crack growth (FCG) tests were conducted in air at room temperature on a servo-hydraulic test machine (MTS)

having a load capacity of 10 tones with a fraquency of 5 Hz under constant amplitude loading. These tests were conducted at constant stress ratio R as indicated Table 4. FCG test using CT specimen under mode I was performed according to ASTM E647 [8]. Precracking for CT specimen was introduced under mode I loading with a sinusoidal wave form, using stress ratio R of 0.1 and a frequency of 10 Hz. The stress intensity factor range during precracking was followed by periodically decreasing the load range in steps of not more than 10 %. a versus N data plotted for CT specimens under constant loading amplitude ,where a and N are the crack length

and number of cycles respectively. Stress- intensity range corresponding to a given crack growth rate calculated from the following expressions. Seven point Incremental Polynomial Method used to plot da/dN versus ΔK.

$$\Delta K = \frac{\Delta P}{B\sqrt{W}} \frac{(2+\alpha)}{(1-\alpha)^{\frac{3}{2}}} (0.886 + 4.64\alpha - 13.32\alpha^2 + 14.72\alpha^3 - 5.6\alpha^4)$$

Where $\alpha = a/W$

Table 4: Fatigue test conditions.

Loading type	Mode I (CT specimen)
Frequency	5
Stress ratio	0.1
Wave form	Sine
Loading angle (°)	0

Results and discussion

Fracture toughness test results

After introducing a fatigue precrack which meets requirements of ASTM E399-09$^{\varepsilon 2}$, MTS 632.01 displacement gage attached to the machined integral knife edges. After attachment of displacement gage, specimen is loaded with loading rate of 0.5 KN/s until specimen fractures. During loading of the specimen, force versus crack mouth opening displacement (CMOD) was recorded by a computerized data acquisition system. Using data, fracture toughness values calculated shown in Table 5. There are two requirements stated in the standard to validity whether calculated KQ value is plane-strain Fracture toughness K_{IC} or not. The first one is the ratio of P_{max}/ P_Q does not exceed ratio 1.1. The latter one is the value 2.5 $(K_Q /\boldsymbol{\sigma}_y)^2$ must be less than the specimen ligament size, W-a.

Table 5a: Fracture toughness R350 HT

Specimen No	Fracture Toughness K_Q $Mpa\sqrt{m}$	Plane –Strain Fracture Toughness K_{IC} $Mpa\sqrt{m}$
HEAD	42.2	42.2
WEB	68.1	---
FOOT	43.4	43.4

Table 5b: Fracture toughness R260 results

Specimen No	Fracture Toughness K_Q $Mpa\sqrt{m}$	Plane –Strain Fracture Toughness K_{IC} $Mpa\sqrt{m}$
HEAD	34.1	34.1
WEB	44.1	---
FOOT	46.7	46.7

By consideration of validity requirement mentioned for plane-strain fracture toughness two specimens in R350 HT and two specimens in R260 meet validity requirement as seen in Table 5.Web specimens which do not meet validity requirement have ligament size w-a less than the value of validity requirement 2.5 $(K_Q /\boldsymbol{\sigma}_y)^2$ therefore calculated values are K_Q Fracture Toughness and not K_{IC} Plane –Strain Fracture Toughness.

Fatigue crack growth rate test results

Crack growth rate versus stress intensity range for all of the specimens are plotted Figure 5 to 7 using seven point incremental polynomial method as given in ASTM E647-11. In this method a second order polynomial is fitted to the seven data points. The local fit has the form like the equation below:

$$\hat{a_i} = b_0 + b_1 \left(\frac{Ni - C1}{C2}\right) + b_2 \left(\frac{Ni - C1}{C2}\right)^2$$

Where $-1 \leq \left(\frac{Ni-C1}{C2}\right) \leq 1$

b_0, b_1 and b_2 are the parameters which are found by least square methods over the range $a_{i-n} \leq a \leq a_{i+n.}$ The growth rate of crack at cycle N_i is calculated by taking the derivative of the fitted parabola as follows:

$$(da/dn)_{\hat{a}i} = (b_1)/(C_2) + 2b_2(N_i - C_1)/C_2^2$$

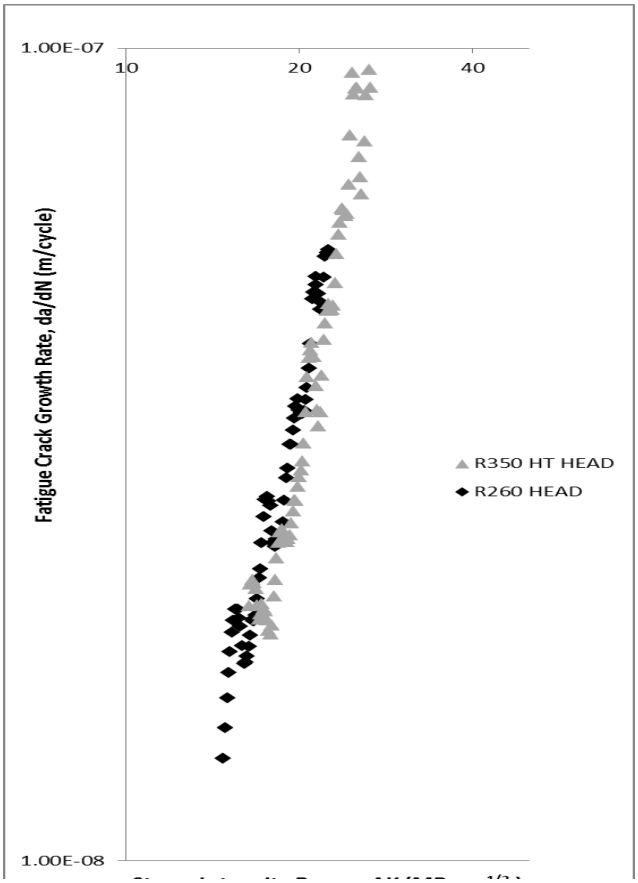

Figure 5:Comparison of da/dN vs.ΔK plot of R350 HT HEAD versus R260 HEAD

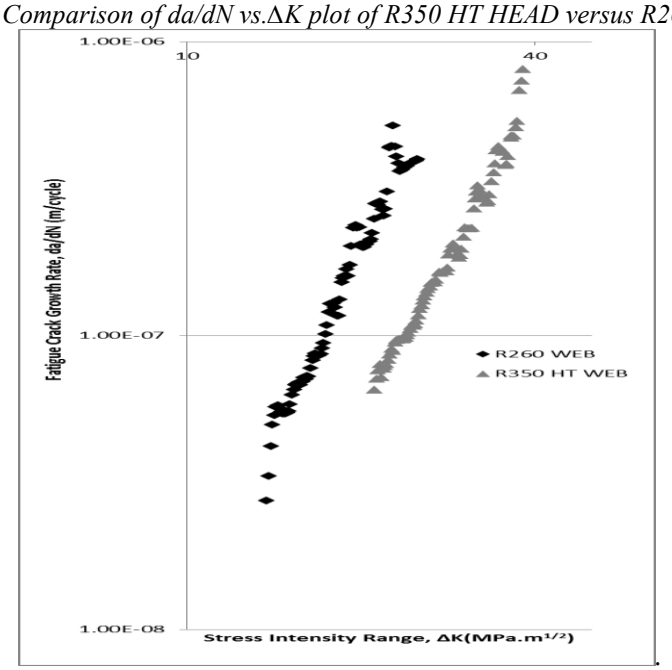

Figure 6: Comparison of da/dN vs.ΔK plot of R350 HT WEB versus R260 WEB.

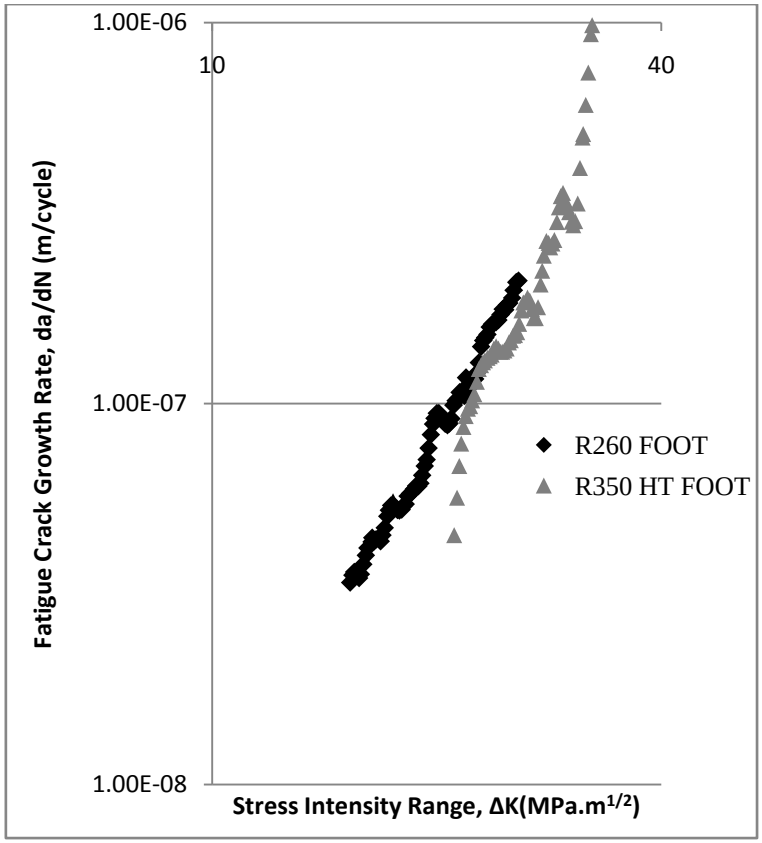

Figure 7: Comparision of da/dN vs ΔK plot of R350 HT FOOT versus R260 FOOT.

Paris-Erdogan law was fit to the linear portion of the plot da/dN versus ΔK of R350 HT and R260 rails. Results of the constants C and m tabulated in Table 6. After determination of constants, rate of fatigue crack growth rate for all specimens calculated at ΔK=25 MPa.$m^{1/2}$as seen in Table 7.

Table 6: Results of the constants C and m.

Specimen No	C	m	R^2
R350HT HEAD	$2.525X10^{-13}$	3.91	0.94
R350HT WEB	$1.004X10^{-12}$	3.62	0.97
R350HT FOOT	$5.034X10^{-14}$	4.62	0.91
R260 HEAD	$1.64X10^{-13}$	4.1	0.95
R260 WEB	$1.78X10^{-13}$	4.66	0.95
R260 FOOT	$6.42X10^{-13}$	3.91	0.97

Table 7: Mode I fatigue crack growth rate data at ΔK = 25 MPa.m1/2.

Specimen No	da/dN(m/cycle)	Stress Ratio (R)
R350HT HEAD	$7.406X10^{-8}$	0.1
R350HT WEB	$1.161X10^{-7}$	0.1
R350HT FOOT	$1.447X10^{-7}$	0.1
R260 HEAD	$8.928X10^{-8}$	0.1
R260 WEB	$5.818X10^{-7}$	0.1
R260 FOOT	$1.891X10^{-7}$	0.1

As seen in Table 7, Fatigue resistance of R350 HT HEAD specimen in transverse direction is higher than web and foot specimens. Furthermore, Fatigue crack growth resistance of web is higher than foot specimen in the same direction.

R260 HEAD specimen in transverse direction has more fatigue crack growth resistance than those of web and foot specimens. Furthermore, fatigue crack growth resistance of foot is higher than web specimen in the same direction.

When the fatigue crack propagation of two rails R350 HT and R260 compared in the head in transverse direction fatigue crack growth resistance of R350 HT is a little bit higher than that of R260, yet it is not so pronounced. It might be concluded that R350 HT and R260 have nearly same fatigue crack propagation in the head of rail.

Comparing web specimens of fatigue crack propagation of two rails R350 HT and R260 in the transverse direction, it is clear from Table 7 and Figure 6 that R350 HT specimen is more resistant than R260 specimen. This difference between fatigue crack propagation rates at the rail web can be correlated to the value of fracture toughness of the web. Since, in the webs of R350 HT and R260 rails, the fracture toughness values are 68.1 $MPa.m^{1/2}$ and 44.1 $MPa.m^{1/2}$ respectively.

Comparing the fatigue crack growth rates of foot specimens of two rails of interest in the transverse direction, at $\Delta K = 25\ MPa.m^{1/2}$ in Table 7, it is apparent that rail R350 HT has more fatigue crack growth resistance than that of R260. But, when looking at the Figure 7 the two da/dN vs ΔK plots behave nearly in the same manner. Furthermore, Paris-Erdogan fit to the linear portion of the plot of da/dN versus ΔK for the foot specimen of R350 HT has lower regression coefficient. Therefore, it may be concluded that due to the reduced of goodness of fit as compared to the other curve fits, calculated *C* and *m* constants are not so reliable for the foot specimen of R350HT.

Electron Fractographic Analysis

The fracture surface of both of the rail R350 HT and R260 were examined under the Scanning Electron Microscope (SEM). Microcrack growth rates of specimens calculated from the fatigue striations at the middle of stage II of propagation. Results of microcrack growth rates are given in Table 8.

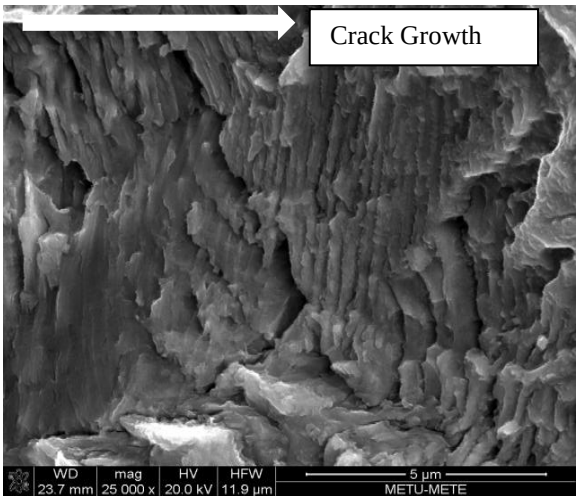

Figure 8: Close view of fatigue striations in the stage II region R350 HT HEAD. (X 25000)

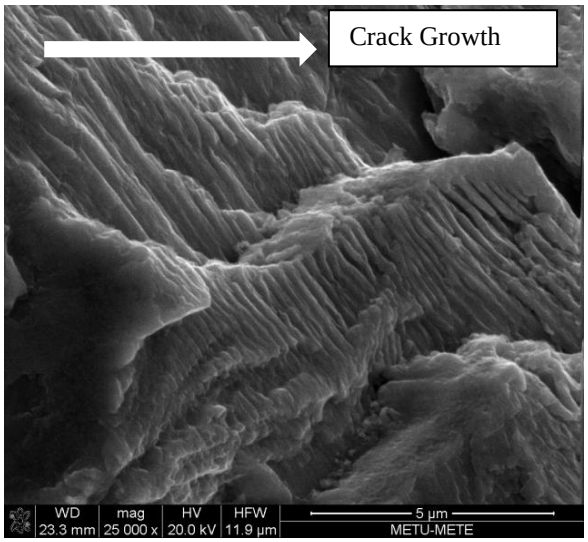

Figure 9: Close view of tear ridges and fatigue striation. (X 25000)

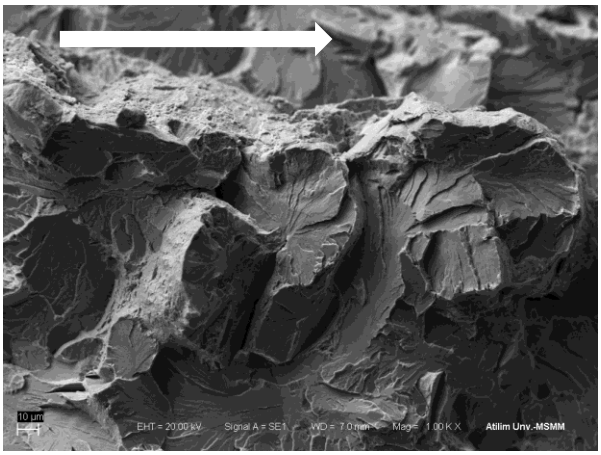

Figure 10: Brittle cleavage final fracture and river markings in each grain. (X 1000)

Table 8: Micro crack growth rate of rail R350 HT and R260.

Specimen No	da/dN(m/cycle)
R350HT HEAD	$2.34X10^{-7}$
R350HT WEB	$2.03X10^{-7}$
R350HT FOOT	$3.00X10^{-7}$
R260 HEAD	$1.87X10^{-7}$
R260 WEB	$3.56X10^{-7}$
R260 FOOT	$3.21X10^{-7}$

From results of table 8 and table 7, it is evident that both of crack propagation rate are consistent nearly to each other.

Conclusions

In this study, fatigue crack propagation of rail R350 HT and R260 under tensile mode in three different region of the 60 kg/m rail steel investigated. From the results of the study it can be said that head hardened rail steels can be replaced with rail R260. The main conclusions drawn from the data are as follwos:

1. Mode I Fracture toughness of R350 HT is higher than that of R260, in the head and the web.
2. Fatigue crack growth resistance of R350 HT in transverse direction is higher in the head as compared to web and foot. Furthermore, fatigue crack growth resistance of web is higher than foot specimen in the same direction.
3. R260 head specimen in transverse direction has greater fatigue crack growth resistance than those of web and foot specimens.
4. Fatigue crack growth resistance of R350 HT is a little bit higher than that of R260, yet it is not so pronounced. It might be concluded that R350 HT and R260 have nearly same fatigue crack propagation rate in the head of rail. Fatigue crack propagation resistance of web of R350 HT in the transverse direction is higher than that of R260 specimen.
5. Fatigue crack growth rates of foot specimens of two rails of interest in the transverse direction are nearly the same.

References

[1]. René Heyder, Gregor Girsch, Testing of HSH® rails in high-speed tracks to minimise rail damage, Wear, Volume 258, Issues 7–8, March 2005, Pages 1014-1021.
[2]. Zerbst U, Lunden R, Edel K. O, Smith R. A. Introduction to the damage tolerance behaviour of railway rails - a review Elsevier: Engineering Fracture Mechanics 2009;76:2563-2601.
[3]. Uwe Zerbst, Stefano Beretta, Failure and damage tolerance aspects of railway components, Engineering Failure Analysis, Volume 18, Issue 2, March 2011, Pages 534-542.
[4]. Ki Myung Lee, Andreas A. Polycarpou, Wear of conventional pearlitic and improved bainitic rail steels, Wear, Volume 259, Issues 1–6, July–August 2005, Pages 391-399.
[5]. Peter Pointner, High strength rail steels—The importance of material properties in contact mechanics problems, Wear, Volume 265, Issues 9–10, 30 October 2008, Pages 1373-1379.

[6]. ASTM E8-04,Standard Test Methods for Tension Testing of Metallic Materials [Metric].
[7]. ASTM E399-09ε2 Standard Test Method for Linear-Elastic Plane-Strain Fracture Toughness *KIc* of Metallic Materials.
[8]. ASTM E647-11 Standard Test Method for Measurement of Fatigue Crack Growth Rates.